Effects of Finite Rate Heterogeneous Kinetics on Homogeneous Ignition in Catalytically Stabilized Channel Flow Combustion

JOHN MANTZARAS* and CHRISTOPH APPEL
Paul Scherrer Institute, Combustion Research, CH-5232 Villigen-PSI, Switzerland

The homogeneous (gas-phase) and heterogeneous (catalytic) ignition of fuel-lean premixtures is investigated analytically and numerically in two-dimensional laminar channel-flow configurations with uniform incoming properties and isothermal catalytic walls. First-order matched activation energy asymptotics are employed, along with a one-step catalytic reaction and a one-step large activation energy gaseous reaction. Parametric description of the chemically frozen state leads to a closed-form heterogeneous ignition criterion in terms of non-dimensional variables that are relevant to confined flows. Formulation of the weakly reactive state yields a closed-form homogeneous ignition criterion that includes explicitly the homogeneous and heterogeneous reactivities through the relevant gaseous and surface Damköhler numbers (Da_g and Da_s, respectively). Both ignition criteria are valid over the range $0.002 \leq x/(bRePr) \leq 0.16$, $1.5 \leq T_W/T_{IN} \leq 3$, and $0.9 \leq Le \leq 2.0$, where x is the streamwise distance, Re the incoming Reynolds number based on the channel half-height b, Pr the Prandtl number, T_W/T_{IN} the wall-to-inlet temperature ratio, and Le the Lewis number of the fuel. Numerical simulations have shown good agreement between the numerically and the analytically predicted homogeneous ignition distances. A reduction of the surface reactivity (Da_s) promotes homogeneous ignition due to the associated increase of the near-wall fuel levels, and this effect is manifested in the homogeneous ignition criterion via a corresponding increase of the characteristic transverse diffusion time scale with decreasing Da_s. It is shown that there exist infinite combinations of surface and gaseous reactivities yielding the same homogeneous ignition distance, suggesting caution in the interpretation of catalytically stabilized combustion (CST) experiments. Moreover, the homogeneous ignition distance is much more sensitive to the gaseous rather than to the surface reaction pathway, thus exemplifying the importance of validated homogeneous reaction schemes under CST-relevant conditions.

NOMENCLATURE

A	Non-dimensional parameter, Eq. 40
b	Channel half-height
B_s, B_g	Frequency factors of surface and gaseous reactions, Eqs. 2 and 3
$\tilde{B}$	Function defined in Eq. A3
c_p	Specific heat at constant pressure
D_i	Species diffusivity
Da_s, Da_g	Surface and gas-phase Damköhler numbers, Eqs. 21 and 46
E_s, E_g	Activation energies of surface and gaseous reactions, Eqs. 2 and 3
f	Non-dimensional stream function, Eq. 14
F	Function defined in Eq. 41
G	Function defined in Eq. 30
H	Function defined in Eq. 42
$I_{h,F}$	Fractional catalytic fuel conversion, Eq. 37
Le	Lewis number ($= Sc/Pr$)
$\dot{m}_{h,F}$, $\dot{m}_{F,IN}$	Catalytic fuel conversion and inlet fuel flow rate, Eqs. 35 and 36
n_i, n	Reaction order ($i = F, O$), sum of reaction orders, Eq. A1
p, p^*	Pressure, non-dimensional pressure
P	Function defined in Eq. 34
Pr	Prandtl number ($= c_p\mu/\lambda$)
q	Heat of combustion per unit mass of fuel
Q	Function defined in Eq. A11
r	Sign-determining exponent in Eqs. 22 and 23
R	Universal gas constant
Re	Reynolds number, Eq. 13
s	Dimensionless streamwise distance, Eq. 12
$\dot{S}_i$	Catalytic reaction rate of species i, Eq. 2

*Corresponding author. E-mail: ioannis.mantzaras@psi.ch

0010-2180/02/$–see front matter
PII S0010-2180(02)00384-X

COMBUSTION AND FLAME 130:336–351 (2002)

Published by Elsevier Science Inc.

Sc	Schmidt number ($= \mu/\rho D$)
T, $\tilde{T}$	Temperature, non-dimensional temperature, Eq. A1
$\tilde{T}_a$	Non-dimensional activation energy, Eq. A1
U_{IN}	Inlet streamwise velocity
u, v	Streamwise and transverse velocity components
W_i, $\bar{W}$	Species molecular weight, average molecular weight
x, y	Streamwise and transverse physical coordinates
Y_i, $\tilde{Y}_i$	Species mass fraction, normalized species mass fraction, Eq. 14
Z	Function defined in Eq. A4

Greek Symbols

α_{th}	Thermal diffusivity ($= \mu/\rho Pr$)
α	Parameter defined in Eq. A14
β	Parameter defined in Eq. A1
γ	Gaseous reaction temperature exponent, Eq. 3
Δ_{cr}, Δ^*_{cr}	Critical and critical ignition Damköhler numbers, Eq. A16
ϵ	Small perturbation parameter, Eq. A6
ζ	Non-dimensional streamwise distance, Eq. 27
η, η^*	Transverse coordinate (Eq. 12), distance at symmetry plane ($y = b$)
θ	Normalized temperature, Eq. 14
λ	Thermal conductivity
μ	Viscosity
ν_i	Species stoichiometric coefficient, Eq. 1
ξ	Normalized transverse coordinate, Eq. A4
ρ	Density
$\tau_{g,ch}$	Characteristic gaseous chemical time, Eq. 44
τ_d	Characteristic transverse diffusion time, Eq. 45
$\tau_{eff,d}$	Effective transverse diffusion time, Eq. 48
ϕ, φ	Equivalence ratio, perturbation parameter for θ
χ	Stretched transverse coordinate, Eq. A6
ψ	Stream function or species perturbation parameter, Eq. A7
ω_i	Species reaction rate, Eq. 16
$\tilde{\omega}$	Non-dimensional reaction parameter, Eq. A2

Subscripts

F, O, P	Fuel, Oxidizer, Product
fr	Chemically frozen
i	Index for species
ig	Ignition
IN	Inlet
inr	Inner solution
s, g	Surface, gas
W	Wall
χ	Differentiation with respect to χ

Superscripts

$'$	Differentiation with respect to η

INTRODUCTION

Catalytically stabilized combustion (CST) provides the best available low-NOx combustion technology for gas turbines (demonstrated NOx emissions less than 3 ppm in small-scale machines [1]), with the added advantage of significant cost reductions compared to competing NOx-aftertreatment techniques such as selective catalytic reduction (SCR) or NOx-storage reduction (SCONOx) [2]. The increased temperature requirements of current generation turbines (up to 1780 K) and the catalyst/substrate thermal stability limitations (acceptable temperatures less than 1400 K) restrict the amount of heterogeneous (catalytic) fuel conversion to about 50%. The catalytic processes, in turn, stabilize via thermal and chemical interactions a subsequent homogeneous (gas-phase) combustion zone, where complete conversion of the remaining fuel and the unburned CO is achieved.

Key issues in CST advancement are the development of ignition catalysts active enough at the relatively low compressor discharge temperatures (ca. 700 K) and the very high spatial velocities of gas turbines, and the attainment of long-term catalyst thermal stability. The former requirement is controlled largely by the physi-

cochemical properties of the fuel/catalyst system, and current research efforts focus on Pd/PdO-based ignition catalysts [3]. Long-term catalyst stability, on the other hand, is controlled primarily by reactor design and not by physicochemical properties. Catalyst operation at the corresponding fuel/air adiabatic flame temperature (corrected appropriately for diffusionally imbalanced fuels [4]) presents an unattainable upper-limit, notwithstanding recent advances in mid- or high-temperature catalyst technology [5]; thermal stability considerations require operation at lower temperatures, and this is achieved with design solutions such as alternate catalytically active/inactive channel coatings [6], diffusional barrier layers [7] for fuels with Lewis number $Le \leq 1$ (e.g., methane), etc. Crucial issues in catalytic reactor design are the attainment of the maximum possible fuel conversion with acceptable pressure drop and without catalyst overheat or initiation of gaseous combustion within the catalytic reactor; the latter event, in particular, can lead to catalyst meltdown.

The delineation of safe operating conditions that ensure no homogeneous ignition inside the catalyst is, therefore, of prime interest in CST. Such information requires the knowledge of validated hetero/homogeneous chemical reaction schemes, the development of multidimensional numerical models incorporating detailed chemistry, and the identification of the key parameters controlling homogeneous ignition. Elementary heterogeneous reaction schemes for the oxidation of simple fuels over Pt and Pd have advanced significantly over the last years [8–11] complementing the extensive literature on gas-phase schemes, and multidimensional CST codes are available nowadays [12, 13]. Furthermore, the validation of various hetero/homogeneous reaction schemes in their capacity to reproduce measured homogeneous ignition characteristics was initiated recently [14, 15]. Analytical homogeneous ignition criteria for channel-flow CST were developed in Mantzaras and Benz [16] using matched activation energy asymptotics, an infinitely-fast catalytic reaction (mass-transport-limited operation), a single-step large activation energy gaseous reaction, and isothermal wall boundary conditions. These criteria were further adapted to atmospheric-pressure CH_4/air CST [17], providing homogeneous ignition distances in good agreement to those predicted numerically using the hetero/homogeneous reaction schemes that were validated in Dogwiler et al. [14]. The aforesaid good agreement is attributed to the fact that, in atmospheric-pressure CH_4/air CST, homogeneous ignition and finite-rate catalytic kinetics are, largely, mutually exclusive events: homogeneous ignition of a hard-to-ignite fuel such as methane requires sufficiently high catalyst and/or inlet temperatures that, in turn, force catalytic operation close to the mass-transport limit.

Finite-rate surface chemistry is, nevertheless, of particular importance under realistic conditions. High-pressure operation exacerbates homogeneous ignition because of the corresponding increase of the gas-phase reactivity of hydrocarbons [18]; homogeneous ignition can, therefore, occur at considerably lower temperatures and therein finite-rate surface kinetics could come to importance. In addition, many combustor designs such as alternate catalytically active/inactive (or active/partially active) coatings, warrant finite-rate surface kinetics on the partially active (or even on the room-temperature inactive) surfaces; finite-rate surface kinetics can, in turn, promote homogeneous ignition due to the associated near-wall fuel excess. Analytical homogeneous ignition studies in catalytic combustion have been reported for external flows, for example, stagnation point flows [19–21] or flat-plate flows [22, 23], and more recently for confined flows [16]. Finite rate surface kinetics were accounted for in the 1-D stagnation-point flow studies [19–21], whereas in the 2-D cases an infinitely-fast surface reaction was considered [22, 23, 16]. Analytical studies in 2-D channel-flow configurations relevant to CST with combined finite-rate surface and gaseous kinetics have not been reported. The present study undertakes an analytical and numerical investigation of isothermal-wall channel CST with main objective to provide closed-form homogeneous ignition criteria that include explicitly the effect of finite-rate surface chemistry. The analysis is based on first order matched activation energy asymptotics in conjunction with the boundary layer approximation, a one-step surface reaction, and a one-step

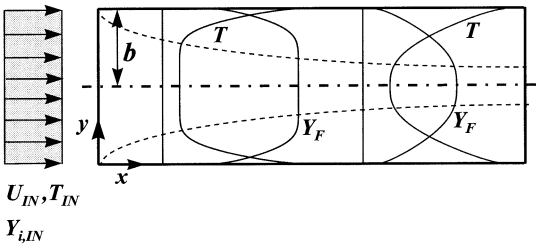

Fig. 1. Plane channel-flow catalytic configuration with uniform inlet properties. Typical transverse (y) profiles of the fuel mass fraction (Y_F) and temperature (T) under finite-rate surface chemistry conditions. The dotted lines mark the extent of the thermal boundary layer.

large activation energy gaseous reaction. Numerical computations are also performed—using the same underlying assumptions as in the analytical work—in order to assess the range of applicability of the analytical solution. Particular objectives are to further establish catalytic ignition criteria for channel-flow CST, and to quantify the sensitivity of homogeneous ignition on both the heterogeneous and the homogeneous reaction pathways; the latter is of particular importance for the validation of hetero/homogeneous reaction schemes with homogeneous ignition investigations [14, 15].

This article is organized as follows. First the mathematical model is given and the parametric description of the chemically frozen state is presented for a first-order (with respect to the deficient reactant) catalytic reaction. The chemically frozen state leads naturally to a heterogeneous ignition criterion. Formulation of the weakly reactive state leads to the corresponding homogeneous ignition criteria. Comparisons between analytically and numerically predicted homogeneous ignition distances follow and, finally, the sensitivity of homogeneous ignition on both reaction pathways is assessed.

MATHEMATICAL FORMULATION

A plane channel configuration with uniform incoming flow properties is considered. It consists of two parallel catalytic plates at a distance $2b$ apart (see Fig. 1), which are maintained at a fixed temperature T_W. A single-step irreversible Arrhenius reaction is considered for both surface and gaseous pathways:

$$[F] + \nu_O[O] \rightarrow \nu_P[P]. \tag{1}$$

To facilitate the ensuing parametric description of the chemically frozen state, a catalytic reaction first-order with respect to the fuel and zero-order with respect to the oxidizer is considered. The surface fuel reaction rate, $\dot{S}_F$, can be expressed as:

$$\dot{S}_F = W_F B_s \left(\frac{\rho Y_F}{W_F}\right)_W \exp\left(-E_s/RT_W\right). \tag{2}$$

The surface rate assumptions are not restrictive for CST since hydrocarbons exhibit first order (with respect to the fuel) global kinetics on precious metal surfaces [24–26].

The gaseous reaction rate has no other restrictions apart from that of a large activation energy. The volumetric gaseous fuel reaction rate, $\dot{\omega}_F$, is:

$$\dot{\omega}_F = W_F B_g T^{\gamma} \left(\frac{\rho Y_F}{W_F}\right)^{n_F} \left(\frac{\rho Y_O}{W_O}\right)^{n_O} \exp\left(-E_g/RT\right). \tag{3}$$

Finite-rate surface kinetics are manifested by the non-zero wall concentration of the deficient reactant (fuel). In the entry flow configuration of Fig. 1, finite-rate surface kinetic effects (increased fuel wall concentrations) are more pronounced at shorter streamwise distances. Under the boundary layer approximation, the governing equations become [27]:

$$\frac{\partial(\rho u)}{\partial x} + \frac{\partial(\rho v)}{\partial y} = 0, \tag{4}$$

$$\rho u \frac{\partial u}{\partial x} + \rho v \frac{\partial u}{\partial y} - \frac{\partial}{\partial y}\left(\mu \frac{\partial u}{\partial y}\right) = -\frac{dp}{dx}, \tag{5}$$

$$\rho u c_p \frac{\partial T}{\partial x} + \rho v c_p \frac{\partial T}{\partial y} - \frac{\partial}{\partial y}\left(\lambda \frac{\partial T}{\partial y}\right) = q\dot{\omega}_F, \tag{6}$$

$$\rho u \frac{\partial Y_i}{\partial x} + \rho v \frac{\partial Y_i}{\partial y} - \frac{\partial}{\partial y}\left(\rho D_i \frac{\partial Y_i}{\partial y}\right) = -\dot{\omega}_i, \tag{7}$$

respectively, with $\partial p/\partial y = 0$. The system of equations is closed with the ideal gas law,

$$p = \rho \frac{R}{\bar{W}} T. \tag{8}$$

The set of Eqs. 4 through 8 constitutes a parabolic system with initial conditions ($x = 0$):

$$u = U_{IN}, \quad v = 0, \quad T = T_{IN}, \quad p = p_{IN},$$
$$\text{and} \quad Y_i = Y_{i,IN}. \tag{9}$$

The boundary conditions at the gas-wall interface ($x > 0$, $y = 0$) are:

$$u = v = 0, \quad T = T_W,$$
$$\text{and} \quad \left(\rho D_i \frac{\partial Y_i}{\partial y}\right)_W = \dot{S}_i. \tag{10}$$

Finally, at the symmetry-plane ($x > 0$, $y = b$) the boundary conditions are:

$$\frac{\partial u}{\partial y} = v = 0, \quad \frac{\partial T}{\partial y} = 0, \quad \text{and} \quad \frac{\partial Y_i}{\partial y} = 0. \tag{11}$$

Relevant to confined flows are the non-dimensional streamwise and transverse coordinates

$$s = x/(bRe) \quad \text{and} \quad \eta = \frac{1}{b\rho_{IN}\sqrt{2s}}\int_0^y \rho \, dy, \tag{12}$$

respectively [16], with Re the inlet Reynolds number based on the channel half-height:

$$Re = \frac{\rho_{IN} U_{IN} b}{\mu_{IN}}. \tag{13}$$

Introducing the stream function $\psi(x, y)$ and the non-dimensional dependent variables,

$$f = \frac{\psi}{b\rho_{IN}U_{IN}\sqrt{2s}}, \quad p^* = \frac{p}{\rho_{IN}U_{IN}^2},$$
$$\theta = \frac{T_W - T}{T_W - T_{IN}}, \quad \tilde{Y}_i = \left(\frac{W_F}{\nu_i W_i}\right) Y_i \tag{14}$$

and assuming equal species diffusivities $D_i = D$, constant values for $\rho\mu$, $\rho\lambda$, $\rho^2 D$, and c_p (resulting in constant Prandtl and Schmidt numbers), the governing Eqs. 4 through 8 become:

$$\frac{\partial^3 f}{\partial \eta^3} + f\frac{\partial^2 f}{\partial \eta^2} + 2s\left(\frac{\partial f}{\partial s}\right)\frac{\partial^2 f}{\partial \eta^2} - 2s\left(\frac{\partial f}{\partial \eta}\right)\frac{\partial^2 f}{\partial \eta \partial s} = 2s\left(\frac{\rho_{IN}}{\rho}\right)\left(\frac{dp^*}{ds}\right) \tag{15}$$

$$Pr^{-1}\frac{\partial^2 \theta}{\partial \eta^2} + f\frac{\partial \theta}{\partial \eta} + 2s\left(\frac{\partial f}{\partial s}\right)\frac{\partial \theta}{\partial \eta} - 2s\left(\frac{\partial f}{\partial \eta}\right)\frac{\partial \theta}{\partial s} = 2s\,\frac{Rebq}{U_{IN}c_p(T_W - T_{IN})}\left(\frac{\dot{\omega}_F}{\rho}\right) \tag{16}$$

$$Sc^{-1}\frac{\partial^2 \tilde{Y}_i}{\partial \eta^2} + f\frac{\partial \tilde{Y}_i}{\partial \eta} + 2s\left(\frac{\partial f}{\partial s}\right)\frac{\partial \tilde{Y}_i}{\partial \eta} - 2s\left(\frac{\partial f}{\partial \eta}\right)\frac{\partial \tilde{Y}_i}{\partial s} = 2s\,\frac{Reb}{U_{IN}}\left(\frac{\dot{\omega}_F}{\rho}\right) \tag{17}$$

$$p = \rho\,\frac{R}{\bar{W}}[T_W - \theta(T_W - T_{IN})]. \tag{18}$$

The initial conditions ($s = 0$) are:

$$f' = 1, \quad \theta = 1, \quad p^* = p^*_{IN}, \quad \frac{1}{\tilde{Y}_{i,IN}}\tilde{Y}_i = 1. \tag{19}$$

Using Eqs. 12, 14, and $\rho_{IN}^2 D_{IN} = \rho_W^2 D_W$, the interfacial ($s > 0$, $\eta = 0$) boundary conditions of Eqs. 10 become:

$$f = 0, \quad f' = 0, \quad \theta = 0,$$

and

$$\frac{1}{\tilde{Y}_{F,IN}}\left(\frac{\partial \tilde{Y}_F}{\partial \eta}\right)_W = Le\,\sqrt{2s}\left(\frac{\rho_W}{\rho_{IN}}\right)\left(\frac{\tilde{Y}_{F,W}}{\tilde{Y}_{F,IN}}\right)Da_s, \tag{20}$$

with Da_s a characteristic surface Damköhler number,

$$Da_s = \frac{bB_s \exp(-E_s/RT_W)}{\alpha_{th,IN}}. \tag{21}$$

Given the equal species diffusivity assumption, the interfacial boundary conditions for species other than fuel are:

$$\left(\frac{\partial \tilde{Y}_i}{\partial \eta}\right)_W = (-1)^r\left(\frac{\partial \tilde{Y}_F}{\partial \eta}\right)_W, \tag{22}$$

with $r = 0$ for the oxidizer and $r = 1$ for the products. Equations 22, under the equal diffusivity assumption, are equivalent to:

$$(\tilde{Y}_{F,W} - \tilde{Y}_{F,IN}) = (-1)^r(\tilde{Y}_{i,W} - \tilde{Y}_{i,IN}). \tag{23}$$

Finally, at the plane-of-symmetry ($s > 0$, $\eta = \eta^*$) the boundary conditions become:

$$f'' = 0, \quad \theta' = 0, \quad \tilde{Y}_i' = 0. \tag{24}$$

For the high inlet Reynolds numbers of CST applications, the boundary layer approximation is valid for purely catalytic combustion [28]; for gaseous combustion it is valid at sufficiently high inlet velocities or low fuel-to-air equivalence ratios [17].

CHEMICALLY FROZEN STATE

Before homogeneous ignition the gas phase is chemically frozen ($E_g/RT_W \to \infty$) and fuel is converted only heterogeneously. Setting $\dot{\omega}_i = 0$, Eqs. 16 and 17 become:

$$Pr^{-1}\frac{\partial^2\theta}{\partial\eta^2} + f\frac{\partial\theta}{\partial\eta} + 2s\left(\frac{\partial f}{\partial s}\right)\frac{\partial\theta}{\partial\eta} - 2s\left(\frac{\partial f}{\partial\eta}\right)\frac{\partial\theta}{\partial s} = 0, \text{ and} \tag{25}$$

$$Sc^{-1}\frac{\partial^2\tilde{Y}_i}{\partial\eta^2} + f\frac{\partial\tilde{Y}_i}{\partial\eta} + 2s\left(\frac{\partial f}{\partial s}\right)\frac{\partial\tilde{Y}_i}{\partial\eta} - 2s\left(\frac{\partial f}{\partial\eta}\right)\frac{\partial\tilde{Y}_i}{\partial s} = 0. \tag{26}$$

The chemically frozen state is formulated by Eqs. 15, 25, 26, and 18, with the initial and boundary conditions given by Eqs. 19, 20, 22, and 24. The set of equations is intrinsically non-similar, necessitating numerical integration with a marching parabolic solver: the numerical procedure is the same as in our previous work [16] and is not repeated. An example of the chemically frozen state is illustrated in Fig. 2 for a propane/air mixture with the global catalytic reaction $C_3H_8 + 5O_2 \to 3CO_2 + 4H_2O$.

Parametric description of the chemically frozen state is sought in terms of the controlling geometrical, flow, transport, and surface-chemistry variables. The quantities necessary for the homogeneous and heterogeneous ignition analysis are the local transverse wall gradients of the temperature and fuel, $\theta'_{fr,W}$ and $(1/\tilde{Y}_{F,IN})(\tilde{Y}'_F)_{fr,W}$, respectively, and the local fuel wall concentration $(1/\tilde{Y}_{F,IN})(\tilde{Y}_F)_{fr,W}$. Closed-form expressions for the aforementioned quantities are presented in terms of a new streamwise coordinate,

$$\zeta = s/Pr = x/(bRePr), \tag{27}$$

which is the inverse of the Graetz number [29]. Computations of the chemically frozen state have recovered the same expression for $\theta'_{fr,W}$ to that of our earlier, mass-transport-limited analysis [16]. $\theta'_{fr,W}$ is a sole function of ζ, Pr and T_W/T_{IN}, and is independent of Da_s:

$$\theta'_{fr,W} = (0.43 + 0.45\zeta^{0.35})\,Pr^{1/3+0.242\zeta^{0.2}} \cdot \left(\frac{T_W}{T_{IN}}\right)^{0.774\zeta^{0.2}}. \tag{28}$$

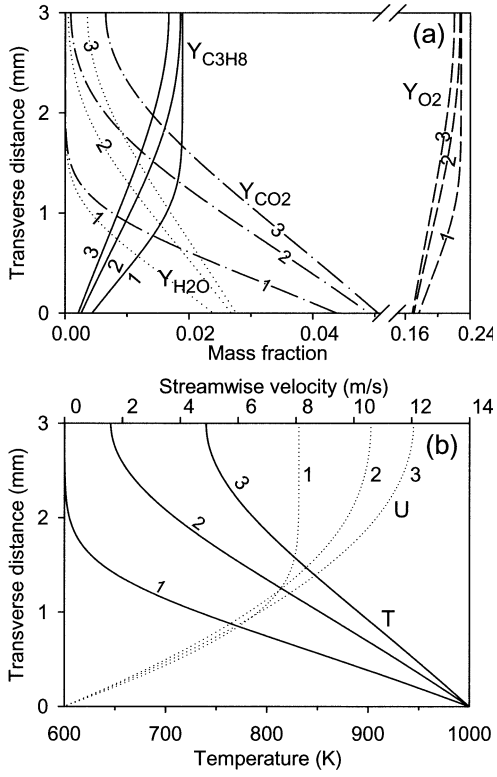

Fig. 2. Computed transverse profiles of the species mass fractions, temperature, and axial velocity at streamwise distances of $x = 19.2$ mm (1), $x = 96$ mm (2), and $x = 192$ mm (3). (a): C_3H_8 (solid lines), H_2O (dotted lines), CO_2 (dashed-dotted lines), and O_2 (dashed lines), (b): temperature (solid lines) and axial velocity (dotted lines). Pure catalytic conversion (gas-phase chemically frozen state) with $\varphi = 0.30$ (propane/air mixture), $T_{IN} = 600$ K, $T_W = 1000$ K, $U_{IN} = 6$ m/s, $p = 1$ bar, $Da_s = 13.2$, and channel half-height $b = 3$ mm.

Under the infinitely-fast surface chemistry assumption, the fuel wall gradient was shown [16] to be a function of ζ, Pr, Le, and T_W/T_{IN}:

$$[(1/\tilde{Y}_{F,IN})(\tilde{Y}'_F)_{fr,W}]_{Da_s\to\infty} = Le^{1/3+0.19\zeta^{0.35}}\theta'_{fr,W}. \tag{29}$$

Equations 28 and 29 are valid over the range $0.002 \le \zeta \le 0.16$, $1.5 \le T_W/T_{IN} \le 3.0$, $0.9 \le Le \le 2.0$ and $0.5 \le Pr \le 1.0$ with accuracy better than 1.6% and 2.5%, respectively.

Inspection of the governing equations and boundary conditions of the chemically frozen state suggests that $(1/\tilde{Y}_{F,IN})(\tilde{Y}'_F)_{fr,W}$ and $(1/\tilde{Y}_{F,IN})(\tilde{Y}_F)_{fr,W}$ are functions of the variables ζ, Pr, Le, T_W/T_{IN}, and Da_s. Defining the function G,

$$G = Le\sqrt{2\zeta Pr}\left(\frac{T_W}{T_{IN}}\right)^{-1}, \tag{30}$$

using Eqs. 8 and 27, and further considering constant $\bar{W}$ and p (the pressure drop is small for $\zeta \leq 0.16$ [29, 16]), the interfacial fuel boundary condition of Eq. 20 can be written as,

$$(1/\tilde{Y}_{F,IN})(\tilde{Y}'_F)_{fr,W} = (1/\tilde{Y}_{F,IN})(\tilde{Y}_F)_{fr,W} G Da_s. \tag{31}$$

Equation 31 links the wall gradient and concentration of the fuel through G and Da_s, which depend solely on the proposed variables of the parametric description; this link is possible only for first-order reactions. Solutions with the following functional dependence are sought:

$$(1/\tilde{Y}_{F,IN})(\tilde{Y}'_F)_{fr,W} = [(1/\tilde{Y}_{F,IN})(\tilde{Y}'_F)_{fr,W}]_{Da_s\to\infty} \cdot \left[\frac{GPDa_s}{GPDa_s + [(1/\tilde{Y}_{F,IN})(\tilde{Y}'_F)_{fr,W}]_{Da_s\to\infty}}\right] \tag{32}$$

and,

$$(1/\tilde{Y}_{F,IN})(\tilde{Y}_F)_{fr,W} = [(1/\tilde{Y}_{F,IN})(\tilde{Y}'_F)_{fr,W}]_{Da_s\to\infty} \cdot \left[\frac{P}{GPDa_s + [(1/\tilde{Y}_{F,IN})(\tilde{Y}'_F)_{fr,W}]_{Da_s\to\infty}}\right], \tag{33}$$

where the function P has to be defined. The fuel wall gradient (Eq. 32) and wall concentration (Eq. 33) expressions satisfy automatically the interfacial boundary condition of Eq. 31. In addition, Eqs. 32 and 33 satisfy the following limiting conditions, provided that $P \to 1$ as $Da_s \to 0$ and $P \cdot Da_s \to \infty$ as $Da_s \to \infty$. In the limit $Da_s \to \infty$, Eqs. 32 and 33 reduce to $(1/\tilde{Y}_{F,IN})(\tilde{Y}'_F)_{fr,W} = [(1/\tilde{Y}_{F,IN})(\tilde{Y}'_F)_{fr,W}]_{Da_s\to\infty}$ and $(1/\tilde{Y}_{F,IN})(\tilde{Y}_F)_{fr,W} = 0$, respectively, that is, to the mass-transport-limited solution; in the limit $Da_s \to 0$, they revert to the chemically inert solution $(1/\tilde{Y}_{F,IN})(\tilde{Y}'_F)_{fr,W} = 0$ and $(1/\tilde{Y}_{F,IN})(\tilde{Y}_F)_{fr,W} = 1$.

Extensive computations have verified the proposed functional dependence: both Eqs. 32 and 33 are within 2.6% of the full numerical predictions, provided that P is:

$$P = 1 + 0.158\left(\frac{T_W}{T_{IN}}\right)^{-1.12} Le^{0.32} Da_s^{0.75} \zeta^{0.13}. \tag{34}$$

Typical streamwise profiles of the fuel wall gradient and fuel concentration are illustrated in Figs. 3 and 4a, respectively. The accuracy of both Eqs. 32 and 33 over the entire allowable range of ζ, T_W/T_{IN}, Le, Pr, and Da_s is illustrated in Fig. 4b.

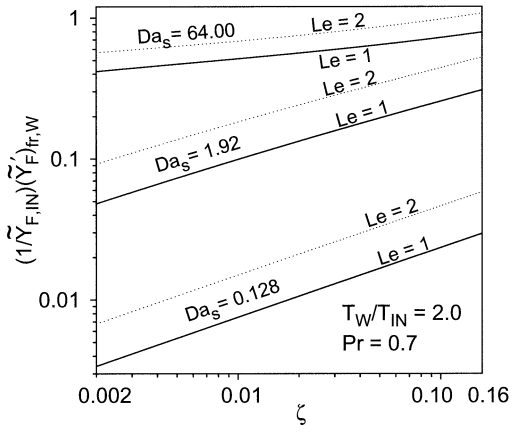

Fig. 3. Chemically frozen state: computed streamwise profiles of the non-dimensional transverse fuel wall gradient for three different surface Damköhler numbers, Da_s, and two Lewis numbers: $Le = 1$ (solid lines) and $Le = 2$ (dotted lines); $Pr = 0.7$ and $T_W/T_{IN} = 2$.

RESULTS AND DISCUSSION

Heterogeneous Ignition

Considering half of the channel domain ($0 \leq y \leq b$), the local integrated heterogeneous fuel conversion rate per unit of channel width is,

$$\dot{m}_{h,F}(x) = \int_0^x \left(\rho D \frac{\partial Y_F}{\partial y}\right)_W dx. \tag{35}$$

The incoming mass fuel flow rate and the integrated fractional catalytic fuel conversion are,

$$\dot{m}_{F,IN} = \rho_{IN} Y_{F,IN} U_{IN} b \quad \text{and}$$

$$I_{h,F}(x) = \dot{m}_{h,F}(x)/\dot{m}_{F,IN}, \tag{36}$$

respectively. Using Eqs. 12, 14, 27, 35, 36, and the relation $\rho_{IN}^2 D_{IN} = \rho_W^2 D_W$, the fractional catalytic fuel conversion becomes:

$$I_{h,F}(\zeta) = \frac{1}{Le}\int_0^\zeta \frac{1}{\sqrt{2Pr\zeta}} (1/\tilde{Y}_{F,IN})(\tilde{Y}'_F)_{fr,W}\, d\zeta. \tag{37}$$

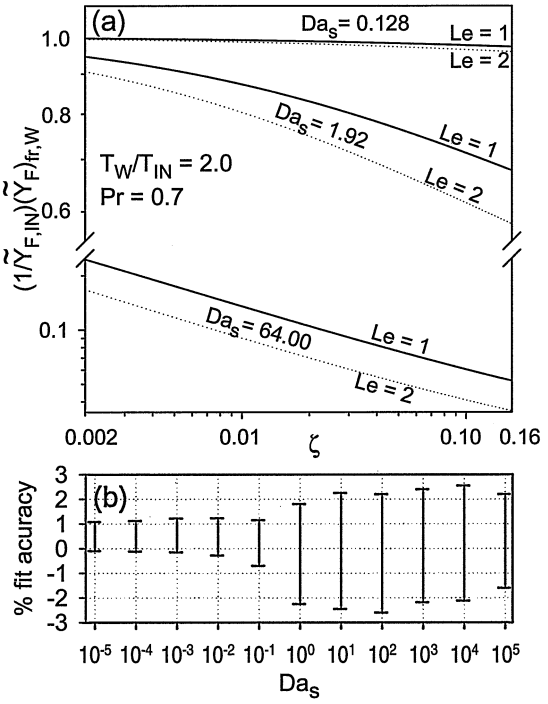

Fig. 4. Chemically frozen state: (a) computed streamwise profiles of the normalized fuel wall concentration for three different surface Damköhler numbers, Da_s, and two Lewis numbers: $Le = 1$ (solid lines) and $Le = 2$ (dotted lines); $Pr = 0.7$ and $T_W/T_{IN} = 2.0$, (b) percentage accuracy (relative to the numerical predictions) of both Eqs. 32 and 33 versus the surface Damköhler number Da_s. The presented bars account for the entire parameter variation $0.002 \leq \zeta \leq 0.16$, $1.5 \leq T_W/T_{IN} \leq 3.0$, $0.9 \leq Le \leq 2.0$ and $0.5 \leq Pr \leq 1.0$.

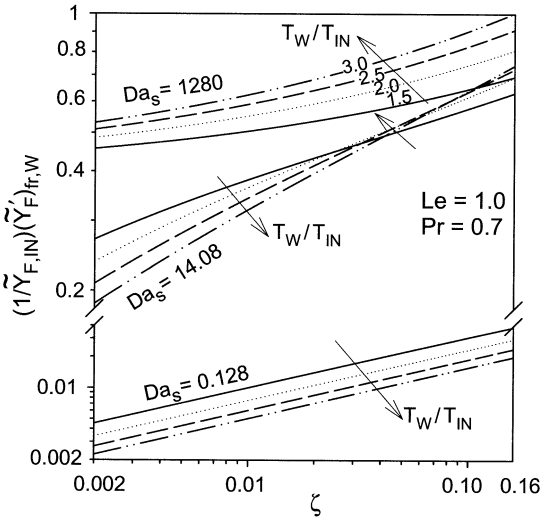

Fig. 5. Chemically frozen state: computed streamwise profiles of the non-dimensional transverse fuel wall gradient $(1/\tilde{Y}_{F,IN})(\tilde{Y}'_F)_{fr,W}$ for various Damköhler numbers Da_s and T_W/T_{IN}: $T_W/T_{IN} = 1.5$ (solid lines), 2.0 (dotted lines), 2.5 (dashed lines), and 3.0 (dashed-doubled dotted lines); $Le = 1.0$ and $Pr = 0.7$. The gradient $(1/\tilde{Y}_{F,IN})(\tilde{Y}'_F)_{fr,W}$ is a decreasing function of T_W/T_{IN} at low Da_s (see $Da_s = 0.128$) and an increasing function of T_W/T_{IN} at high Da_s ($Da_s = 1280$). The arrows indicate the direction of increasing T_W/T_{IN}.

The catalytic conversion (Eq. 37) is directly linked to the fuel wall gradient. For small but non-zero values of Da_s, the fuel wall gradient behaves as $\approx G\, Da_s$ (see Eq. 32), and with the use of Eq. 30, $(1/\tilde{Y}_{F,IN})(\tilde{Y}'_F)_{fr,W} \propto (T_W/T_{IN})^{-1}$, that is, it is a decreasing function of T_W/T_{IN}. At large Da_s, however, $(1/\tilde{Y}_{F,IN})(\tilde{Y}'_F)_{fr,W}$ behaves as $[(1/\tilde{Y}_{F,IN})(\tilde{Y}'_F)_{fr,W}]_{Da_s \to \infty}$, which is a monotonically increasing function of T_W/T_{IN} (see Eqs. 29 and 28). Figure 5 illustrates the aforementioned behavior. At sufficiently high Da_s the surface reactions are fast compared to the fluid mechanical transport. An increase in T_W/T_{IN} through an increase of T_W enhances the transport towards the wall (see Eq. 35 and consider that $\rho_W D_W \propto T_W$ in view of $\rho_W^2 D_W =$ constant). The catalytic reactions can still cope with the increased surface loading, resulting in enhanced catalytic fuel conversion with increasing T_W/T_{IN}. At low Da_s, on the other hand, the surface reactions cannot cope with the increased transport, resulting in a decrease of the catalytic fuel conversion with increasing T_W/T_{IN}. The condition

$$\partial[(1/\tilde{Y}_{F,IN})(\tilde{Y}'_F)_{fr,W}]/\partial(T_W/T_{IN}) = 0 \qquad (38)$$

is, therefore, the appropriate definition of heterogeneous ignition. Equation 38 can be used to define a heterogeneous ignition Damköhler number, $Da_{s,ig}$. Figure 6 demonstrates the calculation of $Da_{s,ig}$ according to the definition of Eq. 38. $Da_{s,ig}$ depends strongly on ζ because finite-rate surface effects are more pronounced at shorter distances.

Of particular interest in practical applications is the attained heterogeneous fuel conversion under finite-rate surface chemistry operating conditions. The ratio of heterogeneous fuel conversion to the corresponding conversion at the mass-transport-limit, $\dot{m}_{h,F}/(\dot{m}_{h,F})_{Da_s \to \infty}$, is presented in Fig. 7. This ratio is bounded between 0.55 and 0.68 over the entire allowable range of ζ, T_W/T_{IN} and Le. In catalysis, heter-

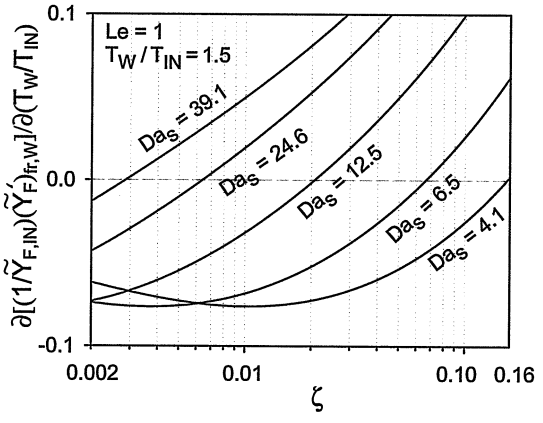

Fig. 6. Calculation of the heterogeneous ignition Damköhler number ($Da_{s,ig}$) for $Le = 1$ and $T_W/T_{IN} = 1.5$. At heterogeneous ignition, the $(1/\tilde{Y}_{F,IN})(\tilde{Y}'_F)_{fr,W}$ versus T_W/T_{IN} profiles have a minimum according to Eq. 38. $Da_{s,ig}$ has a strong dependence on the channel length ζ.

ogeneous ignition is usually defined by the point of 50% relative fuel conversion (compared to the maximum attainable mass-transport-limited conversion), although definitions at relative conversions of 10% or 90% are also common [30, 31]. In this respect, the precise value of the relative fuel conversion at $Da_{s,ig}$ is not of crucial. A simple functional relationship yielding (over the entire range of parameter variation) $Da_{s,ig}$ within 15% to those obtained from Eq. 38 is:

$$Da_{s,ig} = (T_W/T_{IN})^{3/2} Le^{-2/3} \zeta^{-1/2}. \tag{39}$$

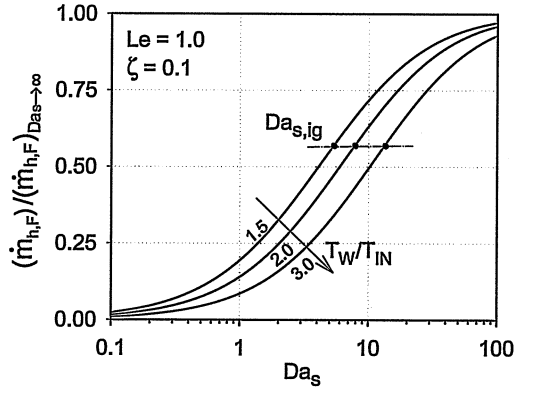

Fig. 7. Computed ratios of catalytic fuel conversion to the maximum attainable mass-transport-limited conversion versus Da_s, for $Le = 1$, $\zeta = 0.1$, and three T_W/T_{IN}. At heterogeneous ignition (calculated from Eq. 38 and shown by the solid points) the ratios $\dot{m}_{h,F}/(\dot{m}_{h,F})_{Da_s\to\infty}$ are about 0.58.

The heterogeneous ignition criterion of Eq. 39 contains all the dependencies on the characteristic flow, transport, chemical and geometrical parameters of the channel-flow configuration. The relation of Eq. 39 could be of interest to mid- or high-temperature CST catalysts that exhibit moderate catalyst temperature variations [32] because of their minimal upstream heat losses. Another application is the steam or CO_2 reforming of CH_4 to synthesis gas over catalysts [33]; the reforming is endothermic, requiring external heating that, in turn, imposes a nearly isothermal catalyst operation. Finally, nearly isothermal wall conditions can be encountered in laboratory-scale burners [14, 15].

Homogeneous Ignition

The asymptotic analysis of the weakly reactive state (details are given in Appendix A) leads to the homogeneous ignition distance, which is obtained from Eqs. A16 and A15. The first bracket of Eq. A16 involves the reactivity and exothermicity of the gaseous reaction; the inverse of this term is defined as:

$$A = \frac{(T_W - T_{IN})^{2+n_F}}{T_W^{2(1+n_F)} (R/E_g)^{1+n_F} (q/c_p)}. \tag{40}$$

Introducing the functions

$$F(\zeta) = \left(\frac{[(1/\tilde{Y}_{F,IN})(\tilde{Y}'_F)_{fr,W}]_{Da_s\to\infty}}{\theta'_{fr,W}} \right)^{n_F} \frac{1}{(\theta'_{fr,W})^2}, \tag{41}$$

and

$$H(\zeta; Da_s) = \frac{[(1/\tilde{Y}_{F,IN})/(\tilde{Y}'_F)]_{Da_s\to\infty}}{GPDa_s}, \tag{42}$$

and further using Eq. 32, the second bracket of Eq. A16 becomes:

$$\left(\frac{(1/\tilde{Y}_{F,IN})(\tilde{Y}'_F)_{fr,W}}{\theta'_{fr,W}} \right)^{n_F} \frac{1}{(\theta'_{fr,W})^2} = F(\zeta) \cdot \left[\frac{1}{1 + H(\zeta; Da_s)} \right]^{n_F}. \tag{43}$$

The third bracket of Eq. A16 is the inverse of a characteristic gaseous reaction time

$$\tau_{g,ch} = [B_g(p\bar{W}/R)^{n_F-1}W_F^{1-n_F}T_W^{1+\gamma-n_F}Y_{F,IN}^{n_F} \cdot \exp(-E_g/RT_W)]^{-1}, \quad (44)$$

and, finally, the last bracket of Eq. A16 after substitution of Eq. 13 becomes a characteristic transverse diffusion time scale:

$$\tau_d = [RePrb/U_{IN}] = b^2/\alpha_{th,IN}. \quad (45)$$

Defining a gas-phase Damköhler number as

$$Da_g = \tau_d/\tau_{g,ch}, \quad (46)$$

substituting Eqs. 41 through 43 in Eq. A16, and solving for the ignition distance ζ_{ig} ($= s_{ig}/Pr$):

$$\zeta_{ig}F(\zeta_{ig}) = \frac{1}{2Pr}A\frac{1}{Da_g}[1 + H(\zeta_{ig}; Da_s)]^{n_F} \cdot \Delta^*_{cr}(\zeta_{ig}; Da_s), \quad (47)$$

with Δ^*_{cr} the critical ignition Damköhler number, obtained from the solution of Eq. A15. The homogeneous ignition criterion of Eq. 47 is valid over the range $0.002 \le \zeta \le 0.16$, $1.5 \le T_W/T_{IN} \le 3.0$, $0.9 \le Le \le 2.0$, and $0.5 \le Pr \le 1.0$.

The main ζ-dependence in Eq. 47 comes from the $\zeta F(\zeta)$ term because of its dominant ζ contribution; moreover, $\zeta F(\zeta)$ is a monotonically increasing function of ζ. For the same T_W, T_{IN}, c_p, and q (e.g., fixed value of A), the right side of Eq. 47 is controlled by the gaseous (Da_g) and surface (Da_s) reactivities. The quantity $[1 + H(\zeta_{ig}; Da_s)]^{n_F}\Delta^*_{cr}(\zeta_{ig}; Da_s)$ is, as further discussed in Appendix B, smaller than unity and decreases monotonically with decreasing Da_s. In conjunction with the aforementioned $\zeta F(\zeta)$ dependence, Eq. 47 implies that homogeneous ignition is favored for either small Da_s or large Da_g. The increased gas-phase reactivity promotes homogeneous ignition directly whereas the reduced surface reactivity promotes ignition indirectly through a larger near-wall fuel excess. In the limit $Da_s \to \infty$, $H(\zeta; Da_s) \to 0$ (see Eq. 42), so that Eq. 47 reduces to the homogeneous ignition criterion $\zeta_{ig}F(\zeta_{ig}) = [\Delta^*_{cr}(\zeta_{ig})]_{Da_s\to\infty}(A/2Pr)(1/Da_g)$ of infinitely fast surface chemistry [16]. For direct comparisons with the mass-transport-limited solution, it is instructive to define an effective transverse diffusion time scale

$$\tau_{eff,d} = \tau_d/[(1 + H(\zeta; Da_s))^{n_F}\Delta^*_{cr}(\zeta; Da_s)/ \cdot [\Delta^*_{cr}(\zeta)]_{Da_s\to\infty}], \quad (48)$$

such that the homogeneous ignition criterion of Eq. 47 can be written equivalently as:

$$\zeta_{ig}F(\zeta_{ig}) = [\Delta^*_{cr}(\zeta_{ig})]_{Da_s\to\infty}(A/2Pr)(\tau_{ch}/\tau_{eff,d}). \quad (49)$$

Under mass-transport-limited conditions, the effective transverse transport time scale $\tau_{eff,d}$ is simply the diffusion time scale τ_d. Finite rate surface kinetics, on the other hand, reduce the transverse transport rates by increasing the effective transverse diffusion time scale (as discussed in Appendix B, the bracketed quantity of Eq. 48 is less or equal to unity and decreases monotonically with decreasing Da_s). To investigate homogeneous ignition, Eq. A15 must solved numerically to provide Δ^*_{cr}; details are provided in Appendix B for a gaseous reaction that is first-order with respect to the fuel ($n_F = 1$).

Sensitivity of Homogeneous Ignition on Surface and Gaseous Reaction Pathways

To assess the importance of each reaction pathway on homogeneous ignition, an application of Eq. 47 is presented next. A propane-oxygen-nitrogen mixture is considered, with incoming composition $Y_{C3H8,IN} = 0.0332$, $Y_{O2,IN} = 0.3764$ ($\phi = 0.32$), and balance nitrogen. The other parameters are $T_{IN} = 600$ K, $p = 1$ bar, $W_F = 44$ kg/kmol, $W_O = 32$ kg/kmol, $\bar{W} = 29$ kg/kmol, $\nu_O = 5$, $q = 46400$ kJ/kgC_3H_8, $c_p = 1.29$ kJ/kgK, $Pr = 0.7$, and $Le = 1.85$. A gaseous reaction first-order with respect to propane and zero-order with respect to oxygen is considered, $(\dot{\omega}_F/W_F) = B_g[C_{C3H8}]\exp(-E_g/RT)$. The activation energy is $E_g = 1.675 \times 10^5$ kJ/kmol [34] and the pre-exponential constant is $B_g = 3.42 \times 10^{10}$ sec^{-1} so that the resulting reaction rate matches the global reaction rate of Westbrook and Dryer [35] proposed for propane flame applications at about 1300 K. It is noted that the above gaseous reaction parameters are intended for the application of Eq. 47 rather than for precise homogeneous ignition calculations in practical systems. Apart

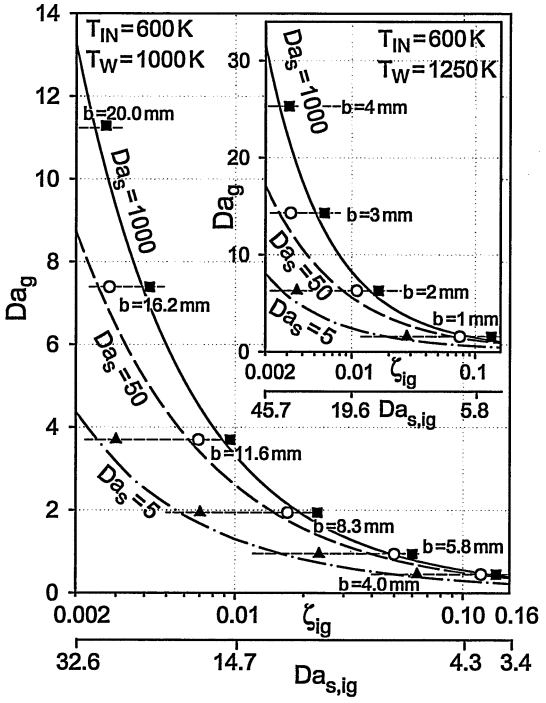

Fig. 8. Homogeneous ignition distances ζ_{ig} versus gaseous Damköhler numbers, Da_g, for a propane-oxygen-nitrogen mixture with $T_{IN} = 600$ K, $T_W = 1000$ K, $p = 1$ bar, $Le = 1.85$, and three different surface Damköhler numbers; the insert figure corresponds to $T_W = 1250$ K. The lines are analytical predictions from Eq. 47 (solid lines $Da_s = 10^3$, dashed lines $Da_s = 50$, and dashed-dotted lines $Da_s = 5$) and the symbols are numerical simulations (solid squares $Da_s = 10^3$, open circles $Da_s = 50$, and solid triangles $Da_s = 5$). The horizontal axes provide also the corresponding heterogeneous ignition Damköhler numbers $Da_{s,ig}$ calculated from the ignition criterion of Eq. 38.

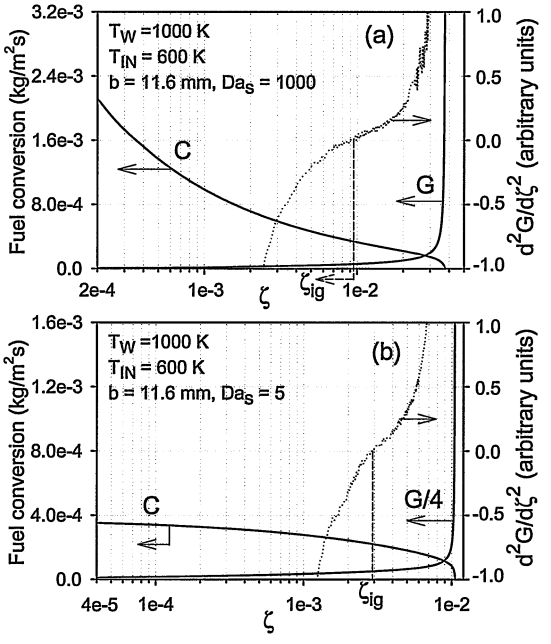

Fig. 9. Computed streamwise profiles of the local catalytic (C) and gaseous (G) fuel conversion rates for $T_{IN} = 600$ K, $T_W = 1000$ K, $b = 11.6$ mm, and two different surface Damköhler numbers: (a) $Da_s = 10^3$ and (b) $Da_s = 5$. For clarity, in (b) the G profile is divided by a factor of four. The onset of homogeneous ignition is defined by the inflection point of the G profile.

from the already known limitations of global steps, accurate homogeneous ignition CST predictions require additional consideration of the hetero/homogeneous coupling of intermediate radical species [14, 15]; in that, a global gaseous reaction should have higher apparent activation energy (compared to that of the purely homogeneous case) to compensate for the inhibition induced by radical adsorption reactions [17].

Plots of non-dimensional ignition distances versus Da_g are presented in Fig. 8 for $T_W = 1000$ K and three different Da_s; $Da_s = 10^3$ is close to the mass-transport-limited solution. The insert of Fig. 8 illustrates the corresponding plots for $T_W = 1250$ K. The lines in Fig. 8 are analytical predictions from Eq. 47 and the symbols are numerical simulations. The definition of homogeneous ignition in the numerical simulations is illustrated in Fig. 9 for $T_{IN} = 600$ K, $T_W = 1000$ K, $b = 11.6$ mm, and two surface reactivities. The local catalytic (C) and gaseous (G) conversions are plotted versus ζ; for direct comparison with the catalytic surface rate, the volumetric gaseous rate has been integrated over the channel half-height. The gaseous conversion rate (G) increases initially very slowly and after a certain streamwise distance that is shorter for the lower Da_s case, it rises exponentially. The inflection point of the G profile ($d^2G/d\zeta^2 = 0$) is used in Fig. 9 to define the onset of homogeneous ignition. The presence of such inflection points can be explained by the competition between fuel depletion and mixture heatup. Initially, $dG/d\zeta$ drops as the near-wall fuel depletion increases with streamwise distance (see Fig. 2a) and at the same time the mixture heating is not yet significant. However, as the thermal effects become important, the Arrhenius exponential dominates and $dG/d\zeta$ increases again. This definition yields ignition

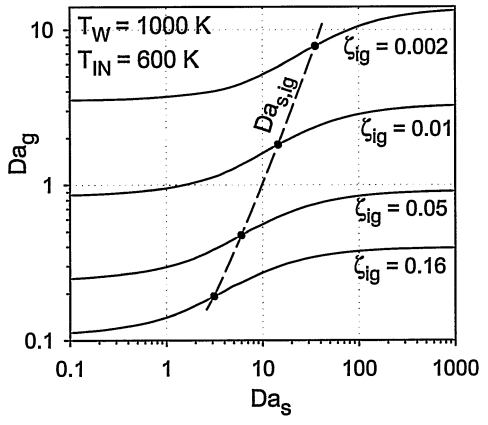

Fig. 10. Lines of constant homogeneous ignition distances (ζ_{ig}) for different combinations of surface and gaseous Damköhler numbers; T_{IN} = 600 K, T_W = 1000 K, the other parameters being as in Fig. 8. The solid points are the heterogeneous ignition Damköhler numbers, $Da_{s,ig}$, calculated from the ignition criterion of Eq. 38.

distances at the base of the rising G-profile, a region where the basic approximations of the mathematical formulation hold, since at the location of the exponential G rise the asymptotic analysis breaks down. In addition, this definition provides ignition distances in good agreement to those predicted analytically. A definition of homogeneous ignition exactly at the point of the exponential G rise would give ζ_{ig} a factor of three larger than those of the analytical predictions; such factors are inherent to all first-order asymptotic analyses for the reasons elaborated in Law and Law [36].

The comparisons between analytical and numerical predictions of Fig. 8 are very favorable. The analytical predictions reproduce not only the trends but also the quantitative features of the numerical predictions. As evidenced from Fig. 8, reduction of Da_s leads to shorter ignition distances ζ_{ig}. Alternately, for a fixed Da_s, reduction of the channel half-height b results in an increase of the ignition distance ζ_{ig}; this is because the surface-to-volume ratio increases with decreasing b and, hence, catalytic conversion is favored against homogeneous conversion. The sensitivity of the ignition distance on both reaction pathways is discussed with the aid of Fig. 10 (referring to the same conditions as Fig. 8), where lines of constant ζ_{ig} are presented for various Da_g and Da_s. As seen from the criterion of Eq. 47 or 49, there are infinite combinations of Da_g and Da_s (such that the terms $Da_g^{-1}[1 + H(\zeta_{ig}; Da_s)]^{n_F}\Delta^*_{cr}(\zeta_{ig}; Da_s)$ or $\tau_{ch}/\tau_{eff,d}$ are constant) that produce the same ζ_{ig}. When a slow surface reaction (e.g., more pronounced near-wall fuel excess) is coupled to a slow gaseous reaction, it can produce the same ζ_{ig} (although not necessarily the same post-ignition flame structure) with that of a faster surface reaction (reduced near-wall fuel excess) coupled to a faster gaseous reaction. The existence of multiple combinations of gaseous and surface reactivities producing the same ζ_{ig} complicates the validation of hetero/homogeneous reaction schemes with homogeneous ignition studies; to circumvent such complications, experimental input is required either on the catalytic processes over the pre-ignition zone or on the flame structure over the post-ignition zone. As seen from Fig. 10, the sensitivity of the homogeneous ignition distance to the surface pathway is more pronounced around $Da_s = Da_{s,ig}$. Even then, ζ_{ig} is most sensitive to the gaseous rather than to the surface pathway; for example, the 10% to 90% rise in Da_g is accomplished by a factor of about 2.5 increase in Da_g (from 0.14 to 0.36 when $\zeta_{ig} = 0.16$ and from 4.5 to 12.3 when $\zeta_{ig} = 0.002$); the corresponding increase in Da_s is much larger (from 0.9–68; e.g., a factor of 75 when $\zeta_{ig} = 0.16$ and from 6 to 327 e.g. a factor of 55 when $\zeta_{ig} = 0.002$). The implications to homogeneous ignition simulations of practical systems are that an uncertainty in the gaseous reaction scheme carries considerably more weight than a corresponding uncertainty in the surface reaction scheme. This is consistent to our recent CST studies of H_2/air mixtures [15], where various elementary hetero/homogeneous reaction schemes were evaluated against measured homogeneous ignition characteristics; there were large differences among the predictions of the various hetero/homogeneous schemes and these differences were ascribed primarily to the gaseous reaction pathway.

CONCLUSIONS

The heterogeneous and homogeneous ignition of fuel-lean premixtures was investigated analytically and numerically in plane channel-flow

configurations with catalytically-active isothermal walls. The following are the key conclusions of this study.

1) A closed-form heterogeneous ignition criterion was derived for a first-order with respect to the fuel global catalytic reaction. The criterion is $Da_{s,ig} = (T_W/T_{IN})^{3/2}\zeta^{-1/2}Le^{-2/3}$, with $Da_{s,ig}$ a corresponding heterogeneous ignition Damköhler number, valid over the range $0.002 \leq \zeta \leq 0.16$, $1.5 \leq T_W/T_{IN} \leq 3.0$, $0.9 \leq Le \leq 2.0$, and $0.5 \leq Pr \leq 1.0$.
2) A closed-form homogeneous ignition criterion was established (Eq. 47), which included explicitly the effect of gaseous and surface reactivities, that is, the relevant Damköhler numbers Da_g and Da_s. The range of applicability of the homogeneous ignition criterion is the same as that of the heterogeneous criterion presented above. Finite-rate rate surface kinetics (decreasing Da_s) promote homogeneous ignition due to the associated increase of the near-wall fuel levels. The effect of finite-rate surface kinetics is manifested in the homogeneous ignition criterion via an increase of the characteristic transverse diffusion time scale with decreasing Da_s.
3) Numerical simulations with fuel-lean propane-oxygen-nitrogen mixtures have shown that, over a wide range of parameter variation, the analytical homogeneous ignition distances are in good agreement with those numerically predicted.
4) The homogeneous ignition distance is much more sensitive to the gaseous rather than to the surface pathway, the reason being that the latter affects homogeneous ignition indirectly via the transport of the deficient reactant (fuel). In addition, there exist infinite combinations of surface and gaseous reactivities (Da_s and Da_g, respectively) yielding the same homogeneous ignition distance, hence suggesting caution in the interpretation of CST experiments.

Support was provided by the Swiss Federal Office of Energy (BFE), Federal Office of Education and Technology (BBT) under contract No. KTI 5344.2 EBS, and Alstom Power Technology of Switzerland.

REFERENCES

1. Beebe, K. W., Cairns, K. D., Pareek, V. K., Nickolas, S. G., Schlatter, J. C., and Tsuchiya, T., *Catalysis Today* 59:95–115 (2000).
2. Forzatti, P., *Appl. Catalysis A: General* 222:221–236 (2001).
3. Farrauto, R. J., Hobson, M. C., Kennelly, T., and Waterman, E. M., *Appl. Catalysis A: General* 81:227–237 (1992).
4. Pfefferle, W. C., and Pfefferle, L. D., *Prog. Energy Combust. Sci*. 12:25–41 (1985).
5. Machida, M., Eguchi, K., and Arai, H., *J. Catalysis* 120:377–386 (1989).
6. Dalla Betta, R., Ribeiro, F. H., Shoji, T., Tsurumi, K., Ezawa, N., and Nickolas, S. G., U.S. Patent No. 5250489, 1993.
7. McCarty, J., Wong, V. L., and Wood, B. J., U.S. Patent No. 6015285, 2000.
8. Hickman, D. A., and Schmidt, L. D., *AIChE* 39(7): 1164–1177 (1993).
9. Deutschmann, O., Schmidt, R., Behrendt, F., and Warnatz, J., *Proc. Combust. Institute* 26:1747–1754 (1996).
10. Hellsing, B., Kasemo, B., and Zhdanov, V. P., *J. Catalysis* 132:210–228 (1991).
11. Aghalayam, P., Park, Y. K., and Vlachos, D. G., *Proc. Combust. Institute* 28:1331–1339 (2000).
12. Dogwiler, U., Benz, P., and Mantzaras, J., *Combust. Flame* 116:243–258 (1999).
13. Deutschmann, O., and Schmidt, L. D., *AIChE* 44(11): 2465–2477 (1998).
14. Dogwiler, U., Mantzaras, J., Benz, P., Kaeppeli, B., Bombach, R., and Arnold, A., *Proc. Combust. Institute* 27:2275–2282 (1998).
15. Appel, C., Mantzaras, J., Schaeren, R., et al., *Combust. Flame* 128:340–368 (2002).
16. Mantzaras, J., and Benz, P., *Combust. Flame* 119:455–472 (1999).
17. Mantzaras, J., Appel, C., and Benz, P., *Proc. Combust. Institute* 28:1349–1357 (2000).
18. Glassman, I., *Combustion*, 3rd Edition. Academic Press, London, 1996, p. 156.
19. Law, C. K., and Sivashinsky, G. S., *Combust. Sci. Technol*. 29:277–286 (1982).
20. Law, C. K., and Chung, S. H., *Combust. Sci. Technol*. 32:307–312 (1983).
21. Trevino, C., *Combust. Sci. Technol*. 30:213–229 (1983).
22. Trevino, C., and Fernandez-Pello, A. C., *Combust. Sci. Technol*. 26:245–251 (1981).
23. Trevino, C., and Peters, N., *Combust. Flame* 61:39–49 (1985).
24. Hiam, L., Wise, H., and Chaikin, S., *J. Catalysis* 9:272–276 (1968).
25. Trimm, D. L., and Lam, C.-W., *Chem. Engineering Sci*. 35:1405–1413 (1980).
26. Markatou, P., Pfefferle, L. D., and Smooke, M. D., *Combust. Flame* 93:185–201 (1993).
27. Williams, F. A., *Combustion Theory*, 2nd Edition. Benjamin/Cummings, CA, 1985, p. 486.
28. Raja, L. L., Kee, R. J., Deutschmann, O., Warnatz, J., and Schmidt, L. D., *Catalysis Today* 59:47–60 (2000).

29. Shah, R. K., and London, A. L., *Laminar Flow Forced Convection in Ducts*. Academic Press, New York, 1978, p. 50.
30. Arnone, S., Busca, G., Lisi, L., Milella, F., Russo, G., and Turco, M., *Proc. Combust. Institute* 27:2293–2299 (1998).
31. Artizzu-Duart, P., Millet, J. M., Guilhaume, N., Garbowski, E., and Primet, M., *Catalysis Today* 59:163–177 (2000).
32. Dalla Betta, R. A., and Rostrup-Nielsen, T., *Catalysis Today* 47:369–375 (1999).
33. Choudhary, V. R., Uphade, B. S., and Mamman, A. S., *Appl. Catalysis A: General* 168:33–46 (1998).
34. Puri, I. K., and Seshadri, K., *Combust. Flame* 65:137–150 (1986).
35. Westbrook, C. K., and Dryer, F. L., *Combust. Sci. Technol*. 27:31–43 (1981).
36. Law, C. K., and Law, H. K., *Combust. Sci. Technol*. 25:1–8 (1981).

Received 9 October 2001; revised 2 April 2002; accepted 19 April 2002

APPENDIX A

Asymptotic Analysis of the Weakly Reactive State

The gaseous reactive state is formulated by Eqs. 15 through 18 with the initial and boundary conditions of Eqs. 19, 20, 23, and 24. In terms of the non-dimensional variables

$$\tilde{T} = \frac{c_p T}{q}, \quad \beta = \frac{\tilde{T}_W - \tilde{T}_{IN}}{\tilde{T}_W},$$

$$\tilde{T}_a = \frac{E_g}{RT_W}, \quad n = n_O + n_F, \tag{A1}$$

$$\tilde{\omega} = (1 - \beta\theta)^{1+\gamma-n} \tilde{Y}_F^{n_F} \tilde{Y}_O^{n_O} \exp\left(\frac{-\tilde{T}_a}{1 - \beta\theta}\right), \tag{A2}$$

$$\tilde{B} = B_g \left(\frac{Reb}{U_{IN}}\right)\left(\frac{p\bar{W}}{RW_F}\right)^{n-1} \nu_O^{n_O} (q/c_p)^{1+\gamma-n} \tilde{T}_W^{1+\gamma-n}, \tag{A3}$$

and the normalized coordinate ξ,

$$\xi = \frac{Z(\eta)}{Z(\eta^*)} \equiv \frac{\displaystyle\int_0^{\eta} \exp\left(-Pr \int_0^{\eta} f\, d\eta\right) d\eta}{\displaystyle\int_0^{\eta^*} \exp\left(-Pr \int_0^{\eta} f\, d\eta\right) d\eta}, \tag{A4}$$

the inner-zone expansion for the temperature, $\theta_{inr} = \theta_{fr} - \epsilon\varphi$, results via an asymptotic matching process (in the same manner as in our earlier mass-transport-limited work [16]) to the following differential equation for the perturbation quantity φ:

$$\frac{d^2\varphi}{d\chi^2} = -2s \frac{\epsilon Pr \tilde{B} \tilde{\omega}}{A_1^2 \beta \tilde{T}_W (\theta'_{fr,W})^2} \tag{A5}$$

with boundary conditions $\varphi(0) = 0$ and $\partial\varphi/\partial\chi = 0$ at $\chi \to \infty$, where

$$\chi = \theta'_{fr,W} \xi Z(\eta^*)/\epsilon \quad \text{and}$$

$$\epsilon = \frac{1}{\beta \tilde{T}_a} = \frac{T_W^2 R}{(T_W - T_{IN}) E_g}. \tag{A6}$$

The asymptotic analysis for the inner-zone of the fuel is discussed next, as it differs from the previous mass-transport analysis [16]. The inner-zone fuel expansion is expressed as:

$$\tilde{Y}_{F,inr} = \tilde{Y}_{F,fr} - \epsilon\psi \tag{A7}$$

with ψ the fuel perturbation. The chemically frozen solution near the wall is

$$(1/\tilde{Y}_{F,IN})\tilde{Y}_{F,fr} = (1/\tilde{Y}_{F,IN})(\tilde{Y}_F)_{fr,W} + (1/\tilde{Y}_{F,IN}) \cdot (\tilde{Y}'_F)_{fr,W}\eta + O(\eta^2). \tag{A8}$$

The temperature and fuel perturbations φ and ψ can be linked as,

$$\psi = \varphi\alpha \frac{(\tilde{Y}'_F)_{fr,W}}{\theta'_{fr,W}}, \tag{A9}$$

where α is to be defined next.

With the aid of Eqs. A6 and A9, the inner-zone expansion of Eq. A7 becomes

$$(1/\tilde{Y}_{F,IN})\tilde{Y}_{F,inr} = \epsilon \frac{(1/\tilde{Y}_{F,IN})(\tilde{Y}'_F)_{fr,W}}{\theta'_{fr,W}} \cdot (Q + \chi - \alpha\varphi). \tag{A10}$$

with

$$Q = \frac{(1/\tilde{Y}_{F,IN})(\tilde{Y}_F)_{fr,W}}{\epsilon[(1/\tilde{Y}_{F,IN})(\tilde{Y}'_F)_{fr,W}/\theta'_{fr,W}]} = \frac{\theta'_{fr,W}}{\epsilon GDa_s}, \tag{A11}$$

Using Eq. A4, the fuel conservation equation (Eq. 17) becomes

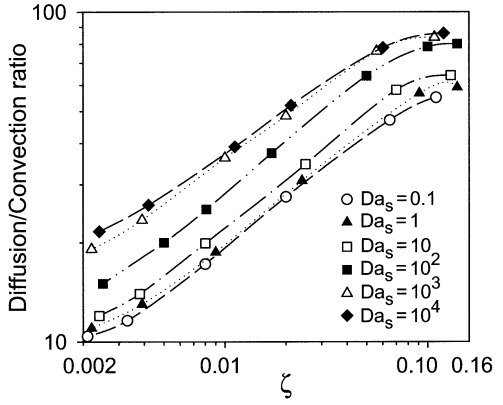

Fig. 11. Numerically predicted ratios of diffusion to streamwise convection (see Eq. A12), at the streamwise position of homogeneous ignition and the transverse location $y/b = 0.005$; $T_W/T_{IN} = 1.67$, $Le = 1.85$, $Pr = 0.7$. The streamwise convection becomes more important at lower Da_s or shorter streamwise distances ζ.

$$Sc^{-1}\frac{\partial^2\tilde{Y}_F}{\partial\xi^2} = 2s\left[\left(\frac{A_2}{A_1}\right)^2\left(\frac{\partial f}{\partial\eta}\right)\frac{\partial\tilde{Y}_F}{\partial s} - \left(\frac{A_2}{A_1}\right)\cdot\left(\frac{\partial f}{\partial s}\right)\frac{\partial\tilde{Y}_F}{\partial\xi}\right] + 2s\left(\frac{A_2}{A_1}\right)^2\frac{\tilde{B}\tilde{\omega}}{\beta\tilde{T}_W}, \tag{A12}$$

with boundary conditions $\tilde{Y}_F = (\tilde{Y}_F)_{fr,W}$ at $\xi = 0$ and $\partial\tilde{Y}_F/\partial\xi = 0$ at $\xi = 1$. The functions A_1 and A_2 are $A_1 = dZ/d\eta$, $A_2 = Z(\eta^*)$. Equation A10 is further substituted in A12 and the leading term balancing the reaction terms is sought. The first convective term on the right side of Eq. A12 deserves attention, notwithstanding its apparent $O(\epsilon^3)$ magnitude, because of the included factor $\partial\tilde{Y}_F/\partial s$. Finite rate surface chemistry can induce large streamwise gradients $\partial\tilde{Y}_F/\partial s$, particularly at short s (or ζ) as shown in Fig. 4. This effect is seen in Fig. 11 where numerically computed diffusion-to-convection ratios, $-[Sc^{-1}\partial^2\tilde{Y}_F/\partial\xi^2]/[2s(A_2/A_1)^2(\partial f/\partial\eta)(\partial\tilde{Y}_F/\partial s)]$, are presented for various Da_s at the streamwise locations of homogeneous ignition and the transverse position $y/b = 0.005$. The gaseous reaction parameters in the computations of Fig. 11 correspond to $\epsilon = 0.12$. A diffusion-to-convection ratio of at least ten is guaranteed even for $Da_s = 0.1$. Consequently, Eq. A12 with the additional use of Eq. A9 reduces to:

$$\frac{d^2\varphi}{d\chi^2} = -2s\frac{\epsilon Sc\tilde{B}\tilde{\omega}}{A_1^2\theta'_{fr,W}(\tilde{Y}'_F)_{fr,W}\alpha}. \tag{A13}$$

The boundary conditions of Eq. A13 are the same with those of Eq. A5. Comparison of Eqs. A13 and A5 shows that $\alpha = Le\beta\tilde{T}_W\theta'_{fr,W}/(\tilde{Y}'_F)_{fr,W}$ and substituting β from Eq. A1,

$$\alpha = \frac{Le(\tilde{T}_W - \tilde{T}_{IN})}{\tilde{Y}_{F,IN}}\left[\frac{\theta'_{fr,W}}{(1/\tilde{Y}_{F,IN})(\tilde{Y}'_F)_{fr,W}}\right]. \tag{A14}$$

Considering—without loss of generality—a gaseous reaction rate that is zero-order with respect to the oxidizer ($n_O = 0$), and substituting Eqs. A2, A6, and A10 into Eq. A13:

$$\frac{d^2\varphi}{d\chi^2} = -\Delta_{cr}(Q + \chi - \alpha\varphi)^{n_F}\exp(\varphi - \chi), \tag{A15}$$

with boundary conditions $\varphi(0) = 0$ and $\partial\varphi/\partial\chi = 0$ at $\chi \to \infty$. Δ_{cr} is the critical ignition Damköhler number, which, under the aforementioned $n_O = 0$ dependence of the gaseous reaction rate, is

$$\Delta_{cr} = 2s\left[\frac{T_W^{2(1+n_F)}(R/E_g)^{1+n_F}(q/c_p)}{(T_W - T_{IN})^{2+n_F}}\right]\cdot\left[\left(\frac{(1/\tilde{Y}_{F,IN})(\tilde{Y}'_F)_{fr,W}}{\theta'_{fr,W}}\right)^{n_F}\frac{1}{(\theta'_{fr,W})^2}\right]\cdot[B_g(p\bar{W}/R)^{n_F-1}W_F^{1-n_F}T_W^{1+\gamma-n_F}Y_{F,IN}^{n_F}\cdot\exp(-E_g/RT_W)][RePrb/U_{IN}]. \tag{A16}$$

APPENDIX B

Critical Ignition Damköhler Numbers

The critical ignition Damköhler number Δ^*_{cr} is determined by the turning point in the wall-gradient perturbation $\varphi_\chi(0)$ versus Δ_{cr} profile; no steady solutions are possible for $\Delta_{cr} > \Delta^*_{cr}$, indicating that the system has undergone thermal runaway. For fixed values of α and Q, numerical integration of Eq. A15 is carried out and the particular value of Δ_{cr} is sought for which a unique solution for the wall gradient $\varphi_\chi(0)$ exists. The calculation of Δ^*_{cr} is illustrated

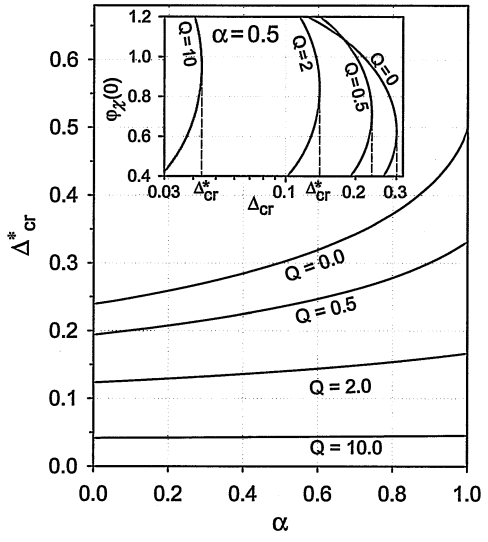

Fig. 12. Computed critical ignition Damköhler numbers Δ^*_{cr} versus α for various values of the parameter Q. In the insert, the calculation of Δ^*_{cr} is illustrated from plots of $\varphi_\chi(0)$ versus Δ_{cr} for $\alpha = 0.5$ and four values of Q.

in the insert of Fig. 12: computed plots of $\varphi_\chi(0)$ versus Δ_{cr} are presented for $\alpha = 0.5$; $Q = 0$ is the infinitely fast surface chemistry solution, and larger Q correspond to slower surface chemistry. Figure 12 provides plots of Δ^*_{cr} versus α constructed with the procedure shown in the insert of Fig. 12. At sufficiently large values of Q, Eq. A15 reduces (for $n_F = 1$) to $d^2\varphi/d\chi^2 = -\Delta_{cr} Q \exp(\varphi - \chi)$: its solution $\Delta^*_{cr}(\zeta; Da_s)$ is such that at large Q the product $\Delta^*_{cr}(\zeta; Da_s)Q$ becomes independent of α or Q and approaches the constant value 0.5. As shown in Fig. 12, already at $Q = 10$, the product $\Delta^*_{cr}(\zeta; Da_s)Q$ ranges from 0.42 to 0.45. Over the entire range of ζ, T_W/T_{IN}, Pr, and Le parameter variation, $\Delta^*_{cr}(\zeta; Da_s)$ decreases faster with decreasing Da_s than the function $[1 + H(\zeta; Da_s)]$ increases with decreasing Da_s; in addition, the term $[1 + H(\zeta; Da_s)]\Delta^*_{cr}(\zeta; Da_s)$ is always less than unity and the term $[1 + H(\zeta; Da_s)]\Delta^*_{cr}(\zeta; Da_s)/[\Delta^*_{cr}(\zeta)]_{Da_s\to\infty}$ is less or equal to unity. Considering, for example, a typical for hydrocarbons value of $\epsilon = 0.1$ and using Eqs. 28 and 30, Eq. A11 yields a minimum $Da_s \approx 1.0$ required to achieve $Q = 10$, which corresponds to $\Delta^*_{cr}(\zeta; Da_s) \approx 0.045$ (see Fig. 12); under these conditions Eq. 42 gives $H(\zeta; Da_s) = 1.3$ and hence $[1 + H(\zeta; Da_s)]\Delta^*_{cr}(\zeta; Da_s) \approx 0.1$. Furthermore, for the minimum possible value of $[\Delta^*_{cr}(\zeta)]_{Da_s\to\infty} \approx 0.24$ (see Fig. 12), $[1 + H(\zeta; Da_s)]\Delta^*_{cr}(\zeta; Da_s)/[\Delta^*_{cr}(\zeta)]_{Da_s\to\infty} \approx 0.4$.